



**HAL**  
open science

## Experimental IR study and ab initio modelling of ethylene adsorption in a MFI - type host zeolite

Natalia Zvereva-Loëte, Anthony Ballandras, Guy Weber, Maud Rotger,  
Vincent Boudon

### ► To cite this version:

Natalia Zvereva-Loëte, Anthony Ballandras, Guy Weber, Maud Rotger, Vincent Boudon. Experimental IR study and ab initio modelling of ethylene adsorption in a MFI - type host zeolite. *Molecular Physics*, 2009, 107 (19), pp.2081-2093. 10.1080/00268970903153683 . hal-00519625

**HAL Id: hal-00519625**

**<https://hal.science/hal-00519625>**

Submitted on 21 Sep 2010

**HAL** is a multi-disciplinary open access archive for the deposit and dissemination of scientific research documents, whether they are published or not. The documents may come from teaching and research institutions in France or abroad, or from public or private research centers.

L'archive ouverte pluridisciplinaire **HAL**, est destinée au dépôt et à la diffusion de documents scientifiques de niveau recherche, publiés ou non, émanant des établissements d'enseignement et de recherche français ou étrangers, des laboratoires publics ou privés.



**Experimental IR study and ab initio modelling of ethylene adsorption in a MFI - type host zeolite**

Journal:	<i>Molecular Physics</i>
Manuscript ID:	TMPH-2009-0117.R2
Manuscript Type:	Full Paper
Date Submitted by the Author:	24-Jun-2009
Complete List of Authors:	Zvereva-Loëte, Natalia; CNRS - Universite de Bourgogne, Institut Carnot de Bourgogne Ballandras, Anthony; CNRS-Universite de Bourgogne, Institut Carnot de Bourgogne Weber, Guy; CNRS-Universite de Bourgogne, Institut Carnot de Bourgogne Rotger, Maud; CNRS-Universite de Bourgogne, Institut Carnot de Bourgogne Boudon, Vincent; CNRS-Universite de Bourgogne, Institut Carnot de Bourgogne
Keywords:	Ab initio, FTIR spectroscopy, Modelling, Vibrational analysis
Note: The following files were submitted by the author for peer review, but cannot be converted to PDF. You must view these files (e.g. movies) online.	
paper_zeolite.tex	

1  
2  
3  
4  
5  
6  
7  
8  
9  
10  
11  
12  
13  
14  
15  
16  
17  
18  
19  
20  
21  
22  
23  
24  
25  
26  
27  
28  
29  
30  
31  
32  
33  
34  
35  
36  
37  
38  
39  
40  
41  
42  
43  
44  
45  
46  
47  
48  
49  
50  
51  
52  
53  
54  
55  
56  
57  
58  
59  
60



For Peer Review Only

# Experimental IR study and *ab initio* modelling of ethylene adsorption in a MFI - type host zeolite.

N. Zvereva-Loëte\*, A. Ballandras, G. Weber, M. Rotger\*\*, V. Boudon, J.-M. Simon

Institut Carnot de Bourgogne - UMR 5209 CNRS-Université de Bourgogne,

9, av. Alain Savary, B.P. 47870, F-21078 Dijon Cedex, France.

(00 Month 200x; In final form 00 Month 200x)

Different *ab initio* methods and experimental results are used to investigate the effect of the adsorption of one ethylene molecule on silicalite-1, a MFI type zeolite. We used simplified models to simulate a portion of a straight or sinusoidal channel of silicalite-1 at a quantum level. The calculated absorption spectra of the models are qualitatively in good agreement with the experimental FTIR spectrum of silicalite-1. Additionally we simulate the FTIR spectrum of the isolated ethylene molecule and that of an ethylene molecule in interaction with the above-mentioned zeolite models. Results are discussed depending on the method and specific basis set and compared with experiments and previous molecular dynamics simulations.

*Keywords:* Ab initio, FTIR spectroscopy, Modelling, Vibrational analysis.

## 1 Introduction

Zeolites are adsorbents that belong to a class of microporous aluminosilicates with an open framework structure. They are built based on a three-dimensional framework of  $TO_4$  ( $T = Al, Si$ ) tetrahedra, each oxygen atom being shared between two tetrahedra. The assemblage of these tetrahedra creates a porous structure with regular arrays of openings, channels and/or cavities in which molecules of various sizes can be trapped. Their catalytic and adsorption properties are the basis of the use of zeolites in gas separation [1], catalysis [2–4], and environmental protection [5, 6]. Many experimental and theoretical investigations

---

\*Corresponding author. Email: Natalia.Loete@u-bourgogne.fr

\*\*Present address: GSMA, CNRS UMR 6089 Moulin de la Housse B.P. 1039 Cases 16-17 F-51687 REIMS Cedex 2

1 were carried out to study physicochemical properties of zeolites [7–27].

2  
3 Fourier Transform Infrared (FTIR) spectroscopy is a powerful technique to investigate adsorption pro-  
4 cesses and particularly the state of physisorbed molecules [8, 9, 18, 28, 29]. Modifications of the spectra  
5 of both the adsorbent and the adsorbate are observed experimentally during physisorption processes. The  
6 interpretation of these modifications is still challenging and needs a theoretical support. Infrared experi-  
7 mental and molecular dynamics (MD) simulation studies were previously jointly performed to characterize  
8 the interaction of ethylene on silicalite-1 at room temperature [5, 8, 29]. The three main results are: (i)  
9 a good agreement between experiment and simulation, (ii) the vibrational response accounts for a global  
10 interaction between the whole structure of the zeolite and ethylene, indicating that the adsorbed ethylene  
11 molecule is not localized on a preferable silicalite site and (iii) the  $\nu_{12}$  vibrational band of ethylene exhibits  
12 a small split at high loading attributed to a condensation effect of the adsorbed phase. It can be underlined  
13 that at very low temperature or/and using cumbersome adsorbates, molecules can be preferentially located  
14 at specific sites. In these cases, contrary to what occurs with ethylene, the spectroscopic response will be  
15 the signature of the specific interaction between a site and the molecule.  
16  
17  
18  
19  
20  
21  
22  
23  
24  
25  
26  
27  
28  
29

30 In this paper we report the experimental results of ethylene adsorption on silicalite-1 obtained by means  
31 of a new FTIR chamber. Additionally, we extended our studies to a quantum approach that is supposed  
32 to give a better description of infrared spectra compared to classical MD simulation. However, *ab initio*  
33 quantum calculations are computationally expensive for systems including a lot of electrons as it is for a  
34 unit cell of zeolite. As a consequence, authors considered only a part of a zeolite unit cell representative  
35 of the geometric and electronic environment [30].  
36  
37  
38  
39  
40  
41  
42

43 In this study a double ring (based on 20 T atoms with oxygen atoms linking two single rings to form  
44 a double ring) and a hydrogenated fragment of it were chosen as models. Previous *ab initio* calculations  
45 on different types of zeolites have used smaller fragments than double rings to model the framework  
46 [14, 18, 19, 21–28]. Different levels of theory are used in this study: RHF (Restricted Hartree Fock), DFT  
47 (Density Functional Theory) and MP2 (Second order Møller-Plesset) methods and compared to experi-  
48 mental and MD data. Section 2 is dedicated to the experimental technique. Section 3 deals with the *ab*  
49  
50  
51  
52  
53  
54  
55  
56  
57  
58  
59  
60

1 *initio* calculating methods and results are discussed in Section 4.  
2  
3  
4

## 5 **2 Experiment**

6  
7

### 8 **2.1 Material**

9

10 Silicalite-1, the aluminium-free end member of the MFI type zeolites was used. It was prepared using  
11 tetrapropylammonium bromide as template in fluoride medium at low temperature ( $< 373$  K) by the  
12 Institut de Sciences des Matériaux de Mulhouse (France). As-synthesized, the zeolite was calcined in air at  
13 873 K for 6 hours to ensure that the template was removed and therefore, that the microporous structure  
14 was opened up. Nitrogen adsorption performed on the calcined sample characterized a micropore volume  
15 of  $0.19 \text{ cm}^3 \cdot \text{g}^{-1}$ . Silicalite-1 crystals exhibit plate-like coffin shape morphologies of homogeneous size of  
16 around  $7 \times 3.5 \times 0.05 \text{ }\mu\text{m}^3$ . Ethylene N35 quality gas was purchased from Air Liquide/Alphagaz Company  
17 and used as adsorptive without further purification.  
18  
19  
20  
21  
22  
23  
24  
25  
26  
27

### 28 **2.2 Apparatus and procedures**

29  
30  
31

32 A home built infrared cell was used to investigate in situ the interaction of ethylene with silicalite-1. This  
33 stainless steel cell is operating at room temperature and for pressures ranging from  $10^{-5}$  up to  $10^3$  hPa.  
34 It is composed of two main parts: (i) an optical chamber equipped with two KBr windows and (ii) a heat  
35 chamber where the sample can be activated up to 573 K under vacuum ( $10^{-5}$  hPa). A linear vertical  
36 transfer allows the transport of the sample held in the sample holder from the heat chamber to the  
37 optical cell. The cell was mounted inside a BRUKER Equinox 55 Fourier transform infrared spectrometer  
38 equipped with a Globar light source, a KBr beam splitter and a DTGS detector. All FTIR absorption  
39 spectra were collected at room temperature over the wavenumber range  $400\text{-}4000 \text{ cm}^{-1}$  and were recorded  
40 by averaging of 100 scans with a resolution of  $4 \text{ cm}^{-1}$ .  
41  
42  
43  
44  
45  
46  
47  
48  
49

50 Infrared spectra of the adsorbent (silicalite-1) were performed using both the KBr and self-supporting  
51 wafer techniques in order to characterize accurately strong and weak lattice zeolite vibrational bands,  
52 respectively. All sample and background (collected without zeolite sample) spectra were recorded at room  
53  
54  
55  
56  
57  
58  
59  
60

1 temperature and pressure.

2  
3 Infrared spectrum of the gas adsorptive was collected after 218 hPa of ethylene was introduced in the cell  
4  
5 previously evacuated under  $10^{-5}$  hPa at room temperature. The pressure value was chosen in order to  
6  
7 measure a well defined, unsaturated spectrum within the wavenumber range  $400\text{-}4000\text{ cm}^{-1}$ . The infrared  
8  
9 spectrum of ethylene was ratioed with a reference spectrum of the empty, evacuated optical cell.

10  
11 Infrared spectra of zeolite in contact with ethylene were performed in the cell using powder sample  
12  
13 pressed into thin self-supporting wafers. Before adsorption, the zeolite sample held in the sample holder  
14  
15 was degassed under vacuum ( $10^{-5}$  hPa) at room temperature. Adsorption (and desorption) measurements  
16  
17 were carried out by exposing the dehydrated sample to increasing (or decreasing) equilibrium pressures  
18  
19 of ethylene from 15 to  $10^3$  hPa (or inversely), at room temperature. The amounts of ethylene adsorbed  
20  
21 at a given pressure, at the equilibrium, were determined from the sorption isotherm obtained by  
22  
23 thermogravimetry. All spectra of the zeolite in equilibrium with gaseous ethylene at a given pressure were  
24  
25 ratioed to background spectra of the cell without sample at the same pressure. The schematic diagram of  
26  
27 the experimental set-up is shown in the Figure 1.

28  
29  
30  
31  
32 [Insert Figure 1 about here]

### 39 3 Computational Procedures

40  
41  
42 All *ab initio* calculations were performed using the Gaussian03 package [31] on a Linux system. We per-  
43  
44 formed three different types of calculations.

45  
46 • The RHF method with a split-valence 3-21G\*\* basis set, that includes -d and -p polarization functions,  
47  
48 was applied to a  $\text{Si}_{20}\text{O}_{50}$  cluster of silicalite. This method has been shown to produce good results for  
49  
50 silicate structures [32]. The compromise between the reliability of the results and the computational cost  
51  
52 is optimized with this basis set. It is important to notice that quantum chemical calculations at this level  
53  
54 of theory overestimate the strength of the chemical bonds. Therefore, a scaling factor is commonly applied  
55  
56  
57  
58  
59  
60

1 to correct the calculated vibrational harmonic wavenumbers [33]. This method was successfully applied in  
2  
3 the development of the *ab initio* force field for aluminosilicate structures [20]. In our study we consider a  
4  
5  $\text{Si}_{20}\text{O}_{50}$  cluster consisting in two  $\text{Si}_{10}\text{O}_{20}$  rings linked by oxygen atoms. The geometry of the  $\text{Si}_{20}\text{O}_{50}$  struc-  
6  
7 ture was fully optimized in the  $C_1$  point group without any constraint. This is a simplified representation  
8  
9 of a portion of a straight or sinusoidal channel of silicalite-1. The normal modes of the  $\text{Si}_{20}\text{O}_{50}$  cluster were  
10  
11 obtained from vibrational harmonic analysis (anharmonicity correction is negligible for these atoms). This  
12  
13 structure was used to simulate the adsorption of ethylene within the zeolite framework.

14  
15 • In the case of ethylene interaction with silicalite-1, adsorption is mainly due to van der Waals dispersion  
16  
17 interactions. The use of Post-Hartree-Fock levels of theory that account for electron correlation leads to  
18  
19 more accurate *ab initio* calculations. The choice of the basis sets is also important. Møller-Plesset pertur-  
20  
21 bation theory (MP2 - MP4) and coupled-cluster methods with all single and double excitations followed  
22  
23 by a perturbative treatment of triple excitations (CCSD(T)) are known to be appropriate for studying van  
24  
25 der Waals complexes and molecular systems. But it should be noticed that these methods require signifi-  
26  
27 cant computational resources for large systems. They are presently intractable for the double ring system.  
28  
29 Therefore, the second order Møller-Plesset perturbation theory MP2 and a more extended split-valence  
30  
31 6-31++G(2d) basis set with diffusion functions on heavy and hydrogen atoms and polarization functions  
32  
33 on heavy atoms was applied to only a small part of the  $\text{Si}_{20}\text{O}_{50}$  model, namely,  $\text{Si}_4\text{O}_{12}\text{H}_8$  (hydrogen atoms  
34  
35 are added to saturate the dangling bonds).

36  
37  
38 • Density Functional Theory (DFT) methods with a hybrid functional in which the exchange energy is  
39  
40 combined with the exact energy from Hartree-Fock theory, provide a reasonable alternative to *ab initio*  
41  
42 methods in predicting geometries, frequencies and energies of van der Waals systems. For zeolites, DFT  
43  
44 methods produce ground state interaction energies that are often correct. The following DFT methods have  
45  
46 been used in our study for the  $\text{Si}_4\text{O}_{12}\text{H}_8$  fragment: B3LYP/6-31++G(2d), MPW1PW91/6-31++G(2d),  
47  
48 PBE1PBE/6-31++G(2d) with three, one and without any parameters (“*ab initio*” functional), that define  
49  
50 the hybrid functional, respectively. One of the Generalized Gradient Approximation methods where the  
51  
52 energy functional depends not only on the electron density but also on its gradient, namely TPSS, have  
53  
54  
55  
56  
57  
58  
59  
60

1 been also used. The optimization of the  $\text{Si}_4\text{O}_{12}\text{H}_8$  structure has been performed at these levels of theory.  
2  
3 The potential energy as a function of the distance  $R$  between this fragment and the ethylene molecule was  
4  
5 also examined and the results were compared with calculations performed at the MP2/6-31++G(2d) level  
6  
7 of theory.  
8

9 *Ab initio* calculations were also performed for the ethylene molecule alone. The harmonic and anharmonic  
10  
11 wavenumbers, overtones and combination bands were calculated by RHF/3-21G\*\*, RHF/6-31++G(2d)  
12  
13 and MP2/6-31++G(2d) methods.  
14

15 The relative intensities of vibrational bands calculated at harmonic level using the Gaussian03 package  
16  
17 have been applied for all simulated spectra presented below.  
18  
19

## 20 21 22 4 Results and discussion 23

24  
25 Geometry optimization and frequency calculations were performed for the  $\text{Si}_{20}\text{O}_{50}$  and  $\text{Si}_4\text{O}_{12}\text{H}_8$  models.  
26  
27 The comparison between frequency analysis based on *ab initio* calculations and experimental infrared  
28  
29 spectroscopy allows to test the validity of the different quantum models and approaches. This is a starting  
30  
31 point of a more general investigation concerning the physisorption of a non polar molecule on a microporous  
32  
33 solid.  
34  
35

### 36 37 38 4.1 Silicalite-1 framework modelling 39

40 The structure of silicalite-1 is based on two interlinked channel systems formed by ten oxygen rings with  
41  
42 sinusoidal channels (free circular cross section diameter of 0.54 nm) running in the (010) plane and straight  
43  
44 channels (free elliptic cross section of  $0.575 \times 0.515 \text{ nm}^2$ ) running in the [010] direction [10, 34]. The minimal  
45  
46 and maximal distances between two opposite oxygen atoms of the ten-membered rings are ranging from  
47  
48 0.7985 nm to 0.8406 nm for straight channels and from 0.8061 to 0.8308 nm for sinusoidal channels [10, 34].  
49  
50 The two different channels are perpendicular to each other and generate intersection areas, which have a  
51  
52 diameter of around 0.9 nm. In the orthorhombic framework geometry (Pnma) of silicalite-1 [10, 34], each  
53  
54 silicon atom is surrounded by four oxygen atoms in a tetrahedral conformation; the Si-O bond lengths  
55  
56  
57  
58  
59  
60

1 are on average of about 0.1587 nm and the Si-O-Si and O-Si-O bending angles are ranging from 145.7 to  
2  
3 177.7° and from 107.1 to 111.5°, respectively. In the present study, a double ring model with 20 Si atoms  
4  
5 and 50 O atoms (20T) is first chosen to represent a portion of a straight or sinusoidal channel of silicalite-1  
6  
7 (Figure 2).  
8

9 [Insert Figure 2 about here.]  
10  
11

12  
13 The geometry optimization has been performed using the RHF/3-21G\*\* level of theory. The structure  
14 optimization of the silicalite model was done without any constraints ( $C_1$  symmetry) and for the equilib-  
15 rium geometry ( $S_e$ ), i.e. at the minimum potential energy surface, without vibrational average structure  
16 ( $S_z$ ). The thermal vibration of the atoms might give a deviation from the equilibrium ( $S_e$ ) structure. The  
17 calculated R(Si-O) bond lengths are ranged between 0.161 and 0.162 nm: these values are close to the  
18 experimental average Si-O bond length [10, 34]. The calculated O-Si-O bending angles are 112.5° and  
19 115.8° and are slightly higher than the ones observed by van Koningsveld et al.[10, 34]. The calculated  
20 Si-O-Si bending angles are 137.2° (angle within the ten-membered rings) and 174.0° (angle between the  
21 two ten-membered rings): these values are also not so far to the ones given in Refs. [10, 34]. The distances  
22 between two opposite oxygen atoms of the ten-membered rings equal 0.869 nm. This value is a little higher  
23 than the experimental value given in Refs. [10, 34]. The distance between neighbour Si atoms of a single  
24 ring is 0.301 nm, that is close to published values ([10, 34]). It is the same for the distance between two  
25 opposite oxygen atoms of the double ring that is 0.427 nm. The differences may be ascribed to the opti-  
26 mization method for the structure of the silicalite model. As a remark, the DFT method was not used on  
27 the  $Si_{20}O_{50}$  cluster because of a convergence problem.  
28  
29  
30  
31  
32  
33  
34  
35  
36  
37  
38  
39  
40  
41  
42  
43  
44  
45  
46  
47

#### 48 **4.2 IR spectra of the unloaded MFI zeolite**

49

50 Vibrations of the zeolite framework give rise to characteristic bands in the mid and far infrared regions.  
51 The infrared spectrum of silicalite-1 obtained from self-supporting and KBr pellet techniques exhibited  
52 fundamental bands assigned, according to the classification of Flanigen [35], to: (i) the stretching vibra-  
53  
54  
55  
56  
57  
58  
59  
60

tional bands  $\nu_{as}(\text{O-Si-O})$ ,  $\nu_{as}(\text{Si-O-Si})$ ,  $\nu_s(\text{Si-O-Si})$  and the bending vibrational band  $\delta(\text{O-Si-O})$  located at 1240, 1089, 806 and 442  $\text{cm}^{-1}$ , respectively, (ii) two overtones of fundamental bands located at 2023 and 1892  $\text{cm}^{-1}$ , and (iii) a system of complex bands located at 686, 629, 588, 569 and 548  $\text{cm}^{-1}$ .

Figure 3 shows the experimental infrared spectrum of silicalite-1 in comparison with the simulated spectrum of the  $\text{Si}_{20}\text{O}_{50}$  zeolite model based on the *ab initio* calculations. The calculated wavenumbers give the position of six vibrational band centers. The first three band centers located at 1129, 839 and 391  $\text{cm}^{-1}$  correspond to  $\nu_{as}(\text{Si-O-Si})$ , the  $\nu_s(\text{Si-O-Si})$  and  $\delta(\text{O-Si-O})$ , respectively. The three others located at 710, 654 and 563  $\text{cm}^{-1}$  correspond to vibrations of the ten-membered double ring of the framework structure. The first two bands are of very weak intensity. Normal mode vibrational analysis performed in the harmonic approximation gives only the positions of fundamental wavenumbers. Overtones cannot be obtained at this level of theory. The  $\nu_{as}(\text{O-Si-O})$  fundamental asymmetrical stretching vibrational band is nevertheless not reproduced by this model, may be owing to the fact that it belongs to an other part of the zeolite framework and it will be interesting to check it using more high level of theory. However, additional bands in particular one located at 1017  $\text{cm}^{-1}$ , of rather low intensities in comparison with those of the four strongest vibrational bands located at 1129, 839, 563 and 391  $\text{cm}^{-1}$  (Table 1), are observed for the  $\text{Si}_{20}\text{O}_{50}$  cluster. The simulated spectrum is in rather good agreement, with respect to the vibrational band positions, with the experimental spectrum (Figure 3). Nevertheless, it shows: (i) a blue-shift by 33 and 40  $\text{cm}^{-1}$  of the  $\nu(\text{Si-O-Si})$  symmetric and  $\nu_{as}(\text{Si-O-Si})$  asymmetric stretching vibrational bands, respectively, and (ii) a red-shift by 51  $\text{cm}^{-1}$  of the  $\delta(\text{O-Si-O})$  bending vibrational band (Table 1). Such a change in position of vibrational bands was also observed from MD simulation calculations [8] (Table 1). However, although calculations may be improved to get better absolute results, what is important to consider is the qualitative spectrum differences between the unloaded zeolite and the zeolite containing an amount of adsorbed ethylene. We assume that the shifts do not qualitatively modify the overall evolution of the system.

[Insert Table 1 about here]

1 [Insert Figure 3 about here]

2  
3  
4  
5 From these results, we estimated that the  $\text{Si}_{20}\text{O}_{50}$  double ring model can be used to reproduce qualita-  
6  
7 tively the main vibrational band positions of silicalite-1.  
8  
9

### 10 11 12 4.3 Infrared spectra of ethylene molecule

13  
14  
15 The theoretical study of the infrared spectrum of an isolated ethylene molecule was carried out using  
16  
17 different *ab initio* methods as described in section 3. A large number of theoretical and experimental  
18  
19 studies including high quality *ab initio* calculations have been already performed on the subject [36–43].  
20  
21 All known vibrational energies in  $\text{C}_2\text{H}_4$  ( $X^1A_g$ ) were reported in Ref. [43]. These data were deduced  
22  
23 from high resolution investigations including the rotational structure. Our objective is to explain the  
24  
25 experimental low resolution infrared spectrum of the ethylene molecule when it is adsorbed in the micro-  
26  
27 pores and on the external surface of silicalite-1. Therefore, the fundamental, combination and overtone  
28  
29 vibrational band wavenumbers were first calculated at the MP2/6-31++G(2d) level of theory. The effect  
30  
31 of anharmonicity was taken into account by the method suggested by Barone that is implemented in  
32  
33 Gaussian03 program [6]. Computed harmonic  $\omega$  and anharmonic  $\nu$  wavenumbers are given in Table 2  
34  
35 together with the experimental data obtained by Duncan et al. [37, 38] and Georges et al. [43]. It should  
36  
37 be noticed that only  $\nu_7$ ,  $\nu_9$ ,  $\nu_{10}$ ,  $\nu_{11}$  and  $\nu_{12}$  vibrational modes are IR active for the ethylene molecule. The  
38  
39 averaged absolute deviation (AAD) between the calculated  $\omega_{calc}$  harmonic wavenumbers and experimental  
40  
41 ones [37, 38] is about  $14 \text{ cm}^{-1}$  and averaged deviation (AD) is  $+11 \text{ cm}^{-1}$  (Table 2). The AAD between  
42  
43 the calculated and experimental [43] anharmonic wavenumbers is found to be about  $15 \text{ cm}^{-1}$  and the AD  
44  
45 is about  $+3 \text{ cm}^{-1}$ . These results show an overestimation of both  $\omega$  and  $\nu$  by the MP2 method for most  
46  
47 of the vibrational modes (Table 2). The deviations with respect to the experimental values do not exceed  
48  
49  $23 \text{ cm}^{-1}$  except for the  $\nu_{11}$  vibrational mode that is largely red shifted by  $63 \text{ cm}^{-1}$  (Table 2). Therefore,  
50  
51 we can conclude that the calculated values are in good agreement with the experimental ones. However,  
52  
53 anharmonic correction for  $\nu_{11}$  is rather overestimated at this level of theory that results in a quite big  
54  
55  
56  
57  
58  
59  
60

1 red-shift with respect to the experimental value (Table 2). The calculated and experimental [43] values of  
2  
3 the combination and overtone wavenumbers are reported in Table 3. The AAD is about  $34\text{ cm}^{-1}$  and the  
4  
5 AD is  $-4\text{ cm}^{-1}$ . However, most of vibrational band positions are overestimated. As far as the ethylene  
6  
7 molecule is concerned, we note that this level of theory gives the position of vibrational bands with an  
8  
9 accuracy that is not adapted to high resolution spectroscopy, but it can provide correct shifts between  
10  
11 isolated and adsorbed molecules.  
12

13  
14  
15 [Insert Table 2 about here]  
16

17  
18  
19 [Insert Table 3 about here]  
20  
21

22  
23  
24 The infrared spectrum of ethylene simulated by the MP2 method is shown in Figure 4 along with the  
25  
26 experimental spectrum obtained under a pressure of 218 hPa at room temperature. The assignment and  
27  
28 location of ethylene vibrational bands are reported in Table 4, in comparison with previous molecular  
29  
30 dynamics results [8]. Both quantum and classical calculations show deviations from experimental data,  
31  
32 depending on the vibrational modes. In general the values of the calculated wavenumbers are slightly  
33  
34 higher (blue-shifts) than the experimental ones. However, we considered that the simulated spectrum is in  
35  
36 rather good agreement with the experimental one. Concerning MD simulation, it is worth to notice that  
37  
38 the method is not suited to obtain combination bands.  
39

40 [Insert Figure 4 about here]  
41

42 [Insert Table 4 about here]  
43  
44  
45  
46  
47  
48  
49

#### 50 4.4 Infrared spectra of ethylene adsorbed in silicalite 51

52  
53 *For the  $\text{Si}_{20}\text{O}_{50} / \text{C}_2\text{H}_4$  system*  
54

55 In a first approach, we modelled the effect of the adsorption of one ethylene molecule on the vibrational  
56  
57  
58  
59  
60

bands of the  $\text{Si}_{20}\text{O}_{50}$  zeolite fragment using the *ab initio* RHF/3-21G\*\* method. The optimization of the  $\text{Si}_{20}\text{O}_{50}$  /  $\text{C}_2\text{H}_4$  structure based on minimization of energy at 0 K, was carried out for a relaxed ethylene molecule and a rigid zeolite framework. The optimized configuration is shown in Figure 5. In this case the molecule is localized at the center of the channel and the CC bond axis is oriented along the channel axis. As represented in Figure 5, the distance between the mass center of the molecule and the surface of the double ring amounts to 0.455 nm. This result is in agreement with molecular dynamics simulation calculations [8].

[Insert Figure 5 about here]

The calculated wavenumbers and intensities of the  $\text{Si}_{20}\text{O}_{50}$  zeolite cluster and the  $\text{Si}_{20}\text{O}_{50}$  /  $\text{C}_2\text{H}_4$  system were introduced in the XTDS software program [44] to further simulate the corresponding vibrational spectra at room temperature. The comparison of the simulated spectra shows that the adsorption of one molecule in the double ring induces a red-shift of about 1 or 2  $\text{cm}^{-1}$  and a very small decrease in intensity of the zeolite vibrational bands, over the wavenumber range 250-1500  $\text{cm}^{-1}$  (Figure 6). Such an evolution is in agreement with the experimental results insofar as a red-shift of the fundamental zeolite vibrational bands is also observed during micropore filling (Figure 7). It can be noticed that the vibrational bands of silicalite-1 at zero loading are slightly shifted compared to Figure 3 because of different constraints for the two sample preparations.

[Insert Figure 6 about here]

[Insert Figure 7 about here]

Additional information about the vibrational bands of the ethylene adsorbed in silicalite-1 were obtained from the simulation. The adsorption induces a red-shift from 3 to 10  $\text{cm}^{-1}$  for the stretching and rocking vibrational bands and a blue-shift from 2 to 17  $\text{cm}^{-1}$  for the bending vibrational bands (except for the  $\omega_3$  and  $\omega_6$  vibrational bands) (Table 5). The interaction of the ethylene molecule with the  $\text{Si}_{20}\text{O}_{50}$  cluster induces the splitting of the cluster vibrational band located at 1017  $\text{cm}^{-1}$  (Table 1) into two components at 1011 and 1016  $\text{cm}^{-1}$ . The contribution at 1011  $\text{cm}^{-1}$  is due to a collective mode of the cluster and  $\omega_7$  ethylene vibrations. It is interesting to note that the calculated red-shifts for the  $\nu_9$  and  $\nu_{11}$  vibrational

bands (we assume that  $\Delta\omega$  is the same as  $\Delta\nu$  in the first approximation) are in good agreement with the ones experimentally observed (Figure 8). The position of the  $\nu_9$  and  $\nu_{11}$  vibrational bands does not change with loading up to 8.5 molecules per unit cell (uc). As a remark, the  $\text{Si}_{20}\text{O}_{50} / \text{C}_2\text{H}_4$  system can be compared with silicalite-1 containing about 8 molecules per unit cell. For the  $\nu_{12}$  in plane bending vibrational band the simulated band is blue-shifted by  $4 \text{ cm}^{-1}$  whereas the experimental one is red-shifted by  $8 \text{ cm}^{-1}$  (Figure 9). Such a discrepancy may be corrected by using methods including electron correlation. The  $\nu_7$  vibrational band of the adsorbed phase is also experimentally observed during micropore filling. However, the evolution of this band is not analysed in the present study because it appears as a shoulder of the strongest vibrational bands of silicalite located at  $1089$  and  $1240 \text{ cm}^{-1}$  (Figure 7). Indeed, these two bands cannot be observed because of detector saturation.

[Insert Table 5 about here]

[Insert Figure 8 about here]

[Insert Figure 9 about here]

*For the  $\text{Si}_4\text{O}_{12}\text{H}_8 / \text{C}_2\text{H}_4$  system*

In a second approach, MP2 calculations were performed in order to include the effects of electron correlations. The MP2 method is known to well describe van der Waals dispersion interactions but calculations are in practice too expensive to be applied to large systems. Therefore, the  $\text{Si}_4\text{O}_{12}\text{H}_8$  fragment (Figure 10) was chosen to calculate the interaction potential energy of the fragment with one ethylene molecule. The  $\text{Si}_4\text{O}_{12}\text{H}_8$  and the ethylene molecule structures were separately optimized at the MP2/6-31++G(2d) level of theory. The optimized structure is shown in Figure 11, the obtained values of the bonds lengths and angles are close to those of the  $\text{Si}_{20}\text{O}_{50}$  cluster. As we observed for the  $\text{Si}_{20}\text{O}_{50}$  cluster, the carbon-carbon double bond of the ethylene molecule is parallel to the plane built by the four silicon atoms of the  $\text{Si}_4\text{O}_{12}\text{H}_8$  fragment. The curve of interaction potential energy versus the distance  $R$  between the fragment and the

ethylene molecule shows a pronounced energy minimum ( $D_e = 12.56 \text{ kJ.mol}^{-1}$ ) at  $R = 0.455 \text{ nm}$  (Figure 12).  $R$  is defined as the distance between the middle of the carbon-carbon double bond of ethylene and the middle of the plane built by the four silicon atoms. It may be surprising that its value is the same as the one calculated at the RHF/3-21G\*\* level of theory for the  $\text{Si}_{20}\text{O}_{50}$  cluster. However, it is not worth to put emphasis on this result, which is a coincidence. The distance dependence of the interaction potential energy can be well fitted by one-dimensional Esposti-Werner function or Lennard-Jones potential (see Appendix) as is shown in Figure 12. This is in agreement with the classical MD simulation results, where no electrostatic potential was used because ethylene molecule is a nonpolar molecule and the Lennard-Jones type of potential was applied, that is well suited to simulate this kind of system [8]. On the other hand, the energy curves calculated by the DFT methods do not show any potential minimum and as a consequence, these methods are not suited to investigate physisorption of non polar molecules.

[Insert Figure 10 about here]

[Insert Figure 11 about here]

[Insert Figure 12 about here]

Wavenumber calculations and analyses were then carried out only for the  $\text{Si}_4\text{O}_{12}\text{H}_8 / \text{C}_2\text{H}_4$  system at the MP2/6-31++G(2d) level of theory. Calculated data are given in Table 5. The adsorption process induces modifications of some ethylene molecule vibrational bands: (i) the intensity of the  $\nu_7$  vibrational band is two times decreased, (ii) the appearance of  $\nu_4$  and  $\nu_8$  vibrational bands which are not infrared active in the gas phase, (iii) the  $\nu_{10}$  and  $\nu_{12}$  vibrational bands are red shifted by  $6 \text{ cm}^{-1}$  whereas the other vibrational bands are slightly or not red shifted. It is interesting to note that the red shift calculated for  $\nu_{12}$  vibrational band is very close to the one experimentally observed ( $8 \text{ cm}^{-1}$ ) and to the value calculated by MD simulation ( $4 \text{ cm}^{-1}$ ). Concerning the appearance of  $\nu_4$  and  $\nu_8$  vibrational bands, we can notice that these bands are not experimentally observed. This result indicates that the  $\text{Si}_4\text{O}_{12}\text{H}_8$  fragment,

1 which is a part of the  $\text{Si}_{20}\text{O}_{50}$  cluster, is not well suited to reproduce all interactions that occur during the  
2  
3 adsorption of ethylene in silicalite. On the other hand, the  $\nu_9$  and  $\nu_{11}$  stretching modes were almost not  
4  
5 changed, meaning that chemical bonds are weakly perturbed by the presence of the  $\text{Si}_4\text{O}_{12}\text{H}_8$  fragment.  
6  
7 Concerning the effect of ethylene adsorption on the vibrational bands of the  $\text{Si}_4\text{O}_{12}\text{H}_8$  structure, the  
8  
9 wavenumbers are also shifted to lower values and the intensities are slightly modified in agreement with  
10  
11 experimental results (Table 6).  
12

13  
14  
15 [Insert Table 5 about here]  
16

17  
18  
19 [Insert Table 6 about here]  
20  
21  
22  
23  
24  
25  
26

## 27 5 Conclusion

28  
29  
30 The aim of this study was to investigate by infrared spectroscopy the interaction of ethylene with an  
31  
32 hydrophobic zeolite, silicalite-1. This study was carried out using quantum calculations at different levels  
33  
34 of theory (RHF, MP2, DFT/B3LYP-PBE1PBE-MPW1PW91) conjointly to infrared experiments at room  
35  
36 temperature. Calculations were performed considering a part of a straight or sinusoidal channel of silicalite-  
37  
38 1, either a  $\text{Si}_{20}\text{O}_{50}$  cluster or an hydrogenated fragment of it,  $\text{Si}_4\text{O}_{12}\text{H}_8$ . Particularly, we focussed on the  
39  
40 evolution of the infrared spectra of: (i) ethylene from the gaseous phase to the adsorbed phase and (ii) the  
41  
42 adsorbent from the unloaded to a loaded state. The first step of this work was to choose the appropriate *ab*  
43  
44 *initio* method that accounts for the infrared spectrum of ethylene and that of the cluster free of adsorbate.  
45  
46 For the  $\text{Si}_{20}\text{O}_{50}$  cluster, calculations were carried out using only the RHF/3-21G\*\* level of theory. In  
47  
48 this case, the calculated infrared spectrum is in a rather good agreement, with respect to the position  
49  
50 of vibrational bands, with the experimental infrared spectrum of the unloaded zeolite. Considering the  
51  
52 ethylene molecule, *ab initio* calculations were performed by using different methods. The best agreement  
53  
54 between the calculated and experimental spectra is obtained with the MP2 method. The second step of  
55  
56  
57  
58  
59  
60

1 this work was to calculate the infrared spectrum of the zeolite in interaction with one ethylene molecule  
2  
3 in order to account for the experimental modifications of the vibrational bands of both the adsorbent and  
4  
5 the adsorbate. In the case of the  $\text{Si}_{20}\text{O}_{50}$  cluster (RHF/3-21G\*\*), the adsorption induces a red-shift by  
6  
7 8 and  $10\text{ cm}^{-1}$  for the  $\nu_{11}$  and  $\nu_9$  ethylene vibrational bands, respectively. These red-shifts are due to a  
8  
9 weakening of the CH bonds and are close to the experimental values that are  $12$  and  $11\text{ cm}^{-1}$ , respectively.  
10  
11 However, for the  $\nu_{12}$  in plane bending vibrational mode, the simulated band is blue-shifted whereas the  
12  
13 experimental one is red-shifted. By using the MP2/6-31++G(2d) method for the  $\text{Si}_4\text{O}_{12}\text{H}_8$  fragment this  
14  
15 discrepancy is corrected to a red-shift. However, with this reduced cluster, the  $\nu_{11}$  and  $\nu_9$  stretching modes  
16  
17 of the ethylene molecule are not modified by the adsorption process. These results show the importance  
18  
19 of the choice of both the zeolite model and the level of theory on the spectroscopic response. Concerning  
20  
21 the choice of the level of theory, it should be noticed that the potential energy curve calculated by the  
22  
23 MP2 method, contrary to RHF and DFT methods, shows a pronounced minimum potential due to van der  
24  
25 Waals interactions. As a consequence, this method is suited to study physisorption of ethylene that is a non  
26  
27 polar molecule. At this step of the study, the quantum calculations give new insight in the understanding  
28  
29 of the spectroscopic response due to adsorption phenomena. However, to be more realistic, additional  
30  
31 calculations should be done by exploring in the future the following new ideas:  
32  
33

34 – the MP2 level of theory should be used for (i) the  $\text{Si}_{20}\text{O}_{50}$  cluster and (ii) a cluster representative of  
35  
36 the intersections of straight and sinusoidal channels. This last point is important since the structure of  
37  
38 intersections is different from that of the channels. Moreover, it contributes to one third of all adsorption  
39  
40 sites.  
41

42 – experimentally, silicalite-1 can adsorb up to around 11 molecules per unit cell. Therefore, at high loading,  
43  
44 intermolecular interactions between ethylene molecules play a significant role. This key point means that  
45  
46 we should simulate the adsorption of two or more ethylene molecules.  
47

48 – from MD simulations we have shown that the ethylene molecules [8] are not trapped on specific sites at  
49  
50 298 K. They are very mobile: the self-diffusion coefficient is of the same order of magnitude as in the liquid.  
51  
52 Moreover, they exhibit a wide distribution of orientations, however, narrower than in the liquid because  
53  
54  
55  
56  
57  
58  
59  
60

of the porous texture. As a consequence, *ab initio* calculations should be done on different orientations to account for the adsorption process of ethylene on silicalite-1 at room temperature.

### Acknowledgments

We acknowledge C. Adamo and L. Joubert for useful discussion and for the computer equipment support of the Ecole Nationale Supérieure de Chimie de Paris (ENSCP, UMR 7575 - Laboratoire d'Electrochimie, chimie des interfaces et modélisation pour l'énergie). We also thank L. Manceron for constructive discussions (LADIR, Paris). Support from the Région Bourgogne for the computer equipment of the Institut Carnot de Bourgogne is gratefully acknowledged. We also wish to thank the GDR 3152 "SpecMo" and the GDR 2997 "COMOVI" of the CNRS.

### Appendix : Analytical representation of the $\text{Si}_4\text{O}_{12}\text{H}_8/\text{C}_2\text{H}_4$ potential

The interaction potential between the ethylene molecule and the  $\text{Si}_4\text{O}_{12}\text{H}_8$  fragment is plotted in Figure 12 as a function of  $R$  that is the distance between the mass centers of  $\text{C}_2\text{H}_4$  and  $\text{Si}_4\text{O}_{12}\text{H}_8$ . *Ab initio* data were fitted first to one-dimensional function of Esposti-Werner type [45]:

$$V(R) = [G(R) \exp(-a_1 R - a_2) - T(R) \sum_{i=3}^8 \left(\frac{C_i}{R^i}\right)],$$

where

$$G(R) = \sum_{i=0}^8 (g_i R^i)$$

and

$$T(R) = \frac{1}{2}[1 + \tanh(1 + tR)]$$

is a switching function. The parameters  $a_i, g_i, t, C_i$  are fitted using the modified Levenberg-Marquardt algorithm from the MIN-PACK set of routines for nonlinear least-square fitting. The quality of the one-dimensional fit is very good. In our potential the position of minimum is  $R_e = 0.455$  nm with a well depth ( $D_e$ ) of  $1049 \text{ cm}^{-1}$  (12.56 KJ/mol).

*Ab initio* points were also fitted to function of Lennard-Jones potential with a very good agreement:

$$V(R) = 4\epsilon \left[ \left(\frac{\sigma}{R}\right)^{12} - \left(\frac{\sigma}{R}\right)^6 \right]$$

1 where  $\epsilon$  and  $\sigma$  are the depth of the the potential well and effective interaction diameter (the distance at  
2  
3 which the potential is zero), respectively. The fitted parameters are  $\sigma = 0.3967$  nm and  $\epsilon = 12.7$  kJ/mol  
4  
5 ( $D_e$ ).  
6  
7  
8  
9  
10  
11  
12  
13  
14  
15  
16  
17  
18  
19  
20  
21  
22  
23  
24  
25  
26  
27  
28  
29  
30  
31  
32  
33  
34  
35  
36  
37  
38  
39  
40  
41  
42  
43  
44  
45  
46  
47  
48  
49  
50  
51  
52  
53  
54  
55  
56  
57  
58  
59  
60

For Peer Review Only

## References

- [1] V. Cottier, J.-P. Bellat, and M.-H. Simonot-Grange, *J. Phys. Chem. B* **101**, 4798 (1997).
- [2] R. Barrer, *Zeolites and Clay Minerals as Sorbents and Molecular Sieves* (Academic Press, London, 1978).
- [3] D. W. Breck, *Zeolite Molecular Sieves* (John Wiley & Sons, New York, 1974).
- [4] M. Guisnet and J. -P. Gilson, *Zeolites for Cleaner Technologies* (Imperial College Press, London, 2002).
- [5] G. Weber, J. -P. Bellat, F. Benoit, C. Paulin, S. Limborg-Noetinger, and M. Thomas, *Adsorption* **11**, 183 (2005).
- [6] V. Barone, *J. Chem. Phys.* **122**, 014108 (2005).
- [7] R. A. van Santen, B. van de Graaf and B. Smit, in *Introduction to zeolite science and practice*, edited by H. van Bekkum, E. M. Flanigen, P. A. Jacobs, J. C. Jansen, **137**, 419 (Elsevier Science, New York, 2001).
- [8] V. Bernardet, A. Decrette, J.-M. Simon, O. Bertrand, G. Weber, and J.-P. Bellat, *Mol. Phys.* **102**, 1859 (2004).
- [9] G. Hübner, G. Rauhut, H. Stoll, and E. Roduner, *Phys. Chem. Chem. Phys.* **4**, 3112 (2002).
- [10] H. van Koningsveld and H. van Bekkum, and J. C. Jansen, *Acta Cryst.* **B43**, 127 (1987).
- [11] M. Boronat, C. M. Zicovich-Wilson, A. Corma, and P. Viruela, *Phys. Chem. Chem. Phys.* **1**, 537 (1999).
- [12] E. Kassab and M. Castellá-Ventura, *J. Phys. Chem. B* **109**, 13716 (2005).
- [13] J. T. Fermann, T. Moniz, O. Kiowski, T. J. McIntire, S. M. Auerbach, T. Vreven, and M. J. Frish, *J. Chem. Theory. Comput.* **1**, 1232 (2005).
- [14] J. Limtrakul, T. Nanok, S. Jungsuttiwong, P. Khongpracha, T. N. Truong, *Chem. Phys. Lett.* **349**, 161 (2001).
- [15] R. A. van Santen, *Catal. Today* **38**, 377 (1997).
- [16] A. Khodakov, S. P. Bates, J. Dwyer, C. M. Windsor, and N. A. Burton, *Phys. Chem. Chem. Phys.*

- 1 1, 507 (1999).  
2  
3 [17] W. Panjan and J. Limtrakul, *J. Mol. Struct.* **654**, 35 (2003).  
4  
5 [18] G. Hübner, G. Rauhut, H. Stoll, and E. Roduner, *J. Phys. Chem. B* **107**, 8568 (2003).  
6  
7 [19] K. Bobuatong and J. Limtrakul, *Appl. Catal., A* **253**, 49 (2003).  
8  
9 [20] K. S. Smirnov and D. Bougeard, *Catal. Today* **70**, 243 (2001).  
10  
11 [21] G. Cantele, F. Trani, D. Ninno, M. Cossi, and V. Barone, *J. Phys. : Condens. Matter* **18**, 2349 (2006).  
12  
13 [22] J. M. Vollmer, E. V. Stefanovich, and T. N. Truong, *J. Phys. Chem. B* **103**, 9415 (1999).  
14  
15 [23] D. Zhou, N. He, Y. Wang, G. Yang, X. Liu, X. Bao, *J. Mol. Struct. (Theochem)* **756**, 39 (2005).  
16  
17 [24] J. Limtrakul, P. Khongpracha, S. Jungstittiwong, T. N. Truong, *J. Mol. Catal. A: Chem.* **153**, 155  
18 (2000).  
19  
20 [25] H. Soscún, O. Castellano, and J. Hernández, *J. Phys. Chem. B* **108**, 5620 (2004).  
21  
22 [26] I. P. Zaragoza, J. M. Martínez-Magadán, R. Santamaria, D. Dixon, M. Castro, *Int. J. Quantum Chem.*  
23 **80**, 125 (2000).  
24  
25 [27] J. M. Vollmer and T. N. Truong, *J. Phys. Chem. B* **104**, 6308 (2000).  
26  
27 [28] R. Z. Khaliullin and A. T. Bell, V. B. Kazansky, *J. Phys. Chem. A* **105**, 10454 (2001).  
28  
29 [29] O. Bertrand, G. Weber, S. Maure, V. Bernardet, J. P. Bellat, and C. Paulin, *J. Phys. Chem. B* **109**,  
30 13312 (2005).  
31  
32 [30] P. Sherwood, A. H. de Vries, S. J. Collins, S. P. Greatbanks, N. A. Burton, M. A. Vincent, and I. H.  
33 Hillier, *Faraday Discuss.* **106**, 79 (1997).  
34  
35 [31] M. J. Frisch, G. W. Trucks, H. B. Schlegel, G. E. Scuseria, M. A. Robb, J. R. Cheeseman, J. A.  
36 Montgomery, Jr., T. Vreven, K. N. Kudin, J. C. Burant, J. M. Millam, S. S. Iyengar, J. Tomasi, V.  
37 Barone, B. Mennucci, M. Cossi, G. Scalmani, N. Rega, G. A. Petersson, H. Nakatsuji, M. Hada, M.  
38 Ehara, K. Toyota, R. Fukuda, J. Hasegawa, M. Ishida, T. Nakajima, Y. Honda, O. Kitao, H. Nakai,  
39 M. Klene, X. Li, J. E. Knox, H. P. Hratchian, J. B. Cross, V. Bakken, C. Adamo, J. Jaramillo, R.  
40 Gomperts, R. E. Stratmann, O. Yazyev, A. J. Austin, R. Cammi, C. Pomelli, J. W. Ochterski, P. Y.  
41 Ayala, K. Morokuma, G. A. Voth, P. Salvador, J. J. Dannenberg, V. G. Zakrzewski, S. Dapprich, A. D.  
42  
43  
44  
45  
46  
47  
48  
49  
50  
51  
52  
53  
54  
55  
56  
57  
58  
59  
60

- 1 Daniels, M. C. Strain, O. Farkas , D. K. Malick, A. D. Rabuck, K. Raghavachari, J. B. Foresman,  
2  
3 J. V. Ortiz, Q. Cui, A. G. Baboul, S. Clifford, J. Cioslowski, B. B. Stefanov, G. Liu , A. Liashenko, P.  
4  
5 Piskorz, I. Komaromi, R. L. Martin, D. J. Fox, T. Keith, M. A. Al-Laham, C. Y. Peng, A. Nanayakkara,  
6  
7 M. Challacombe, P. M. W. Gill, B. Johnson, W. Chen, M. W. Wong, C. Gonzalez, J. A. Pople, et al.,  
8  
9 *Gaussian 03, Revision C.02*, Gaussian, Inc., Wallingford, CT, 2004.
- 10  
11 [32] L. J. Criscenti, S. L. Brantley, K. T. Mueller, N. Tsomaia, and J. D. Kubicki, *Geochim. Cosmochim.*  
12  
13 *Acta* **69**, 2205 (2005).  
14
- 15 [33] A. P. Scott and L. Radom, *J. Phys. Chem.* **100**, 16502 (1996).  
16
- 17 [34] H. van Koningsveld, *Acta Cryst.* **B46**, 731 (1990).  
18
- 19 [35] E. M. Flanigen, H. Khatami, and H. A. Szymanski, *Adv. Chem. Ser.* **101**, 201 (1971).  
20
- 21 [36] W. Raballand, M. Rotger, V. Boudon, M. Loëte, J. Breidung, W. Thiel, *J. Mol. Struct.* **780-781**, 70  
22  
23 (2006).  
24
- 25 [37] J. L. Duncan, D. C. McKean, and P. D. Mallinson, *J. Mol. Spectrosc.* **45**, 221 (1973).  
26
- 27 [38] J. L. Duncan and E. Hamilton, *J. Mol. Struct. (Theochem)* **76**, 65 (1981).  
28
- 29 [39] N. Dam, R. Engeln, J. Reuss, A. S. Pine, A. Fayt, *J. Mol. Spectrosc.* **139**, 215 (1990).  
30
- 31 [40] I. Cauuet, J. Walrand, G. Blanquet, A. Valentin, L. Henry, C. Lambeau, M. de Vleeschouwer, and  
32  
33 A. Fayt, *J. Mol. Spectrosc.* **139**, 191 (1990).  
34
- 35 [41] D. V. Lerberghe, I. J. Wright, and J. L. Duncan, *J. Mol. Spectrosc.* **42**, 251 (1972).  
36
- 37 [42] J. M. L. Martin, T. J. Lee, P. Taylor, J.-P. François, *J. Chem. Phys.* **103**, 2589 (1995).  
38
- 39 [43] R. Georges, M. Bach, and M. Herman, *Mol. Phys.* **97**, 279 (1999).  
40
- 41 [44] C. Wenger, V. Boudon, M. Rotger, M. Sanzharov, and J. -P. Champion, *J. Mol. Spectrosc.* **251**, 102  
42  
43 (2008).  
44
- 45 [45] A. D. Esposti and H. J. Werner *J. Chem. Phys.* **93**, 3351 (1990).  
46  
47  
48  
49  
50  
51  
52  
53  
54  
55  
56  
57  
58  
59  
60

## Figure captions

1  
2  
3  
4  
5  
6  
7  
8  
9  
10 Figure 1. Schematic diagram of the experimental set-up: 1 - Sample handler; 2 - Oven; 3 - KBr window; 4 - Indium o-ring; 5 - Sample  
11 holder; 6 - Sample; 7 - Thermocouple.

12  
13  
14 Figure 2. RHF/3-21G\*\* optimized geometry of the  $\text{Si}_{20}\text{O}_{50}$  double ring cluster representative of a portion of a straight or sinusoidal  
15 channel of silicalite-1 (red: oxygen atoms; yellow: silicon atoms).

16  
17  
18 Figure 3. Experimental infrared spectrum of Silicalite-1 (KBr-supported sample wafer) recorded under ambient conditions (continuous  
19 curve). Comparison with the infrared spectrum of the  $\text{Si}_{20}\text{O}_{50}$  cluster calculated at the RHF/3-21G\*\* level of theory (dotted lines).

20  
21  
22 Figure 4. Experimental infrared spectrum of ethylene recorded under a pressure of 218 hPa at room temperature (continuous curve).  
23 Comparison with the spectrum of ethylene calculated at MP2/6-31++G(2d) level of theory.

24  
25  
26 Figure 5. RHF/3-21G\*\* optimized geometry of the  $\text{Si}_{20}\text{O}_{50}/\text{C}_2\text{H}_4$  structure (red: oxygen atoms; yellow: silicon atoms; grey: carbon  
27 atoms; pale grey: hydrogen atoms).

28  
29  
30 Figure 6. Infrared spectra of the  $\text{Si}_{20}\text{O}_{50}$  cluster free of adsorbate (solid curve) and with one adsorbed ethylene molecule (dotted  
31 curve), calculated at the RHF/3-21G\*\* level of theory.

32  
33  
34 Figure 7. Dependence of the experimental infrared spectrum of silicalite-1 (self-supported sample wafer) on ethylene loading: (from  
35 bottom to top) 0.0, 4.3 and 8.5 molecules / uc, at room temperature. In italic also reported the position of two weak vibrational bands  
36 of silicalite-1 and their dependence on loading (values from top to bottom).

37  
38  
39 Figure 8. Dependence of the experimental of the  $\nu_{11}$  and  $\nu_9$  vibrational bands of ethylene adsorbed on silicalite-1 on loading: (from  
40 top to bottom) 0.7, 3.4, 4.3, 5.1, 6.1, 7.3 and 8.5 molecules / uc (left), the corresponding equilibrium pressure in hPa (right).  
41 Comparison with the experimental gas ethylene spectrum (dotted curve).

42  
43  
44 Figure 9. Dependence of the experimental of the  $\nu_{12}$  vibrational band of ethylene adsorbed on silicalite-1 on loading: (from top to  
45 bottom) 0.7, 3.4, 4.3, 5.1, 6.1, 7.3 and 8.5 molecules / uc (left), the corresponding equilibrium pressure in hPa (right). Comparison with  
46 the experimental gas ethylene spectrum (dotted curve).

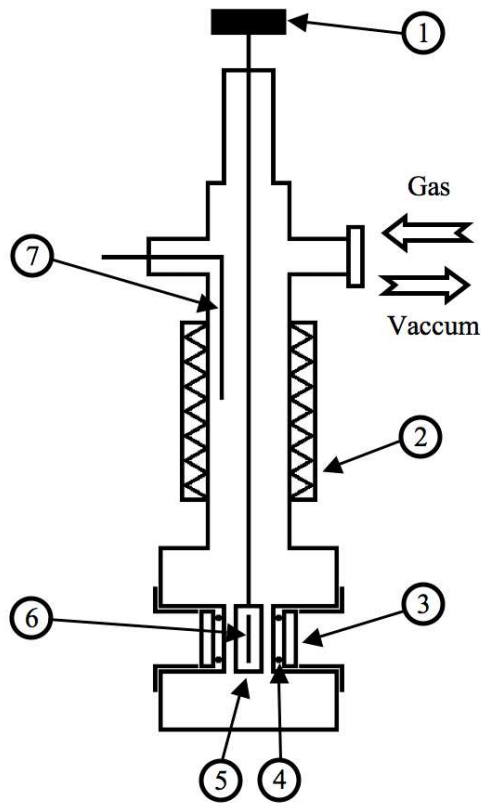
1 Figure 10. MP2/6-31++G(2d) optimized geometry of the  $\text{Si}_4\text{O}_{12}\text{H}_8$  fragment (red: oxygen atoms; yellow: silicon atoms; pale grey:  
2  
3 hydrogen atoms).

4 Figure 11. Geometry of the  $\text{Si}_4\text{O}_{12}\text{H}_8 / \text{C}_2\text{H}_4$  structure at the energy minimum calculated at the MP2/6-31++G(2d) level of theory  
5  
6 (red: oxygen atoms; yellow: silicon atoms; grey: carbon atoms; pale grey: hydrogen atoms).  
7

8  
9 Figure 12. Interaction potential between ethylene molecule and  $\text{Si}_4\text{O}_{12}\text{H}_8$  fragment as a function of the distance between the  
10  
11 geometric centers. Comparison between different calculated models.  
12  
13  
14  
15  
16  
17  
18  
19  
20  
21  
22  
23  
24  
25  
26  
27  
28  
29  
30  
31  
32  
33  
34  
35  
36  
37  
38  
39  
40  
41  
42  
43  
44  
45  
46  
47  
48  
49  
50  
51  
52  
53  
54  
55  
56  
57  
58  
59  
60

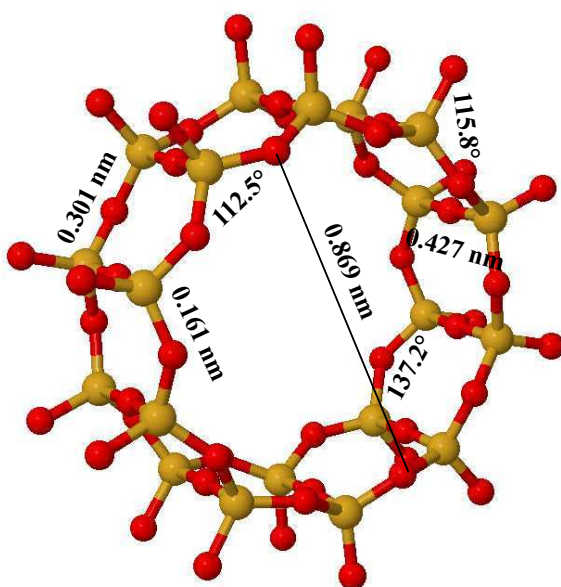
For Peer Review Only

Fig. 1



1  
2  
3  
4  
5  
6  
7  
8  
9  
10  
11  
12  
13  
14  
15  
16  
17  
18  
19  
20  
21  
22  
23  
24  
25  
26  
27  
28  
29  
30  
31  
32  
33  
34  
35  
36  
37  
38  
39  
40  
41  
42  
43  
44  
45  
46  
47  
48  
49  
50  
51  
52  
53  
54  
55  
56  
57  
58  
59  
60

Fig. 2



FC

Only

1  
2  
3  
4  
5  
6  
7  
8  
9  
10  
11  
12  
13  
14  
15  
16  
17  
18  
19  
20  
21  
22  
23  
24  
25  
26  
27  
28  
29  
30  
31  
32  
33  
34  
35  
36  
37  
38  
39  
40  
41  
42  
43  
44  
45  
46  
47  
48  
49  
50  
51  
52  
53  
54  
55  
56  
57  
58  
59  
60

Fig. 3

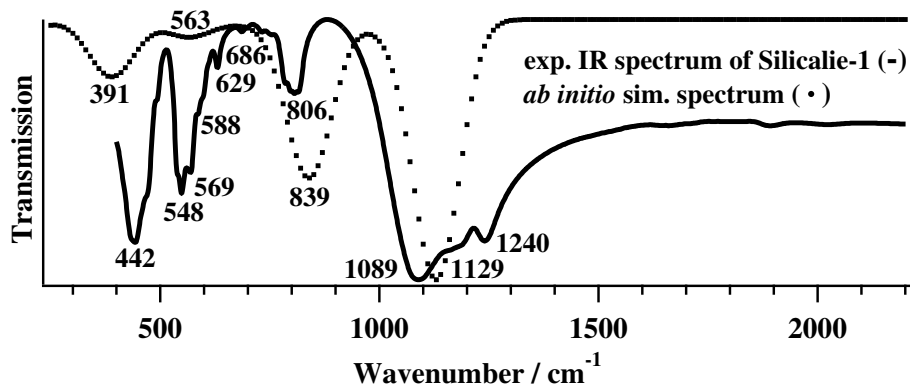
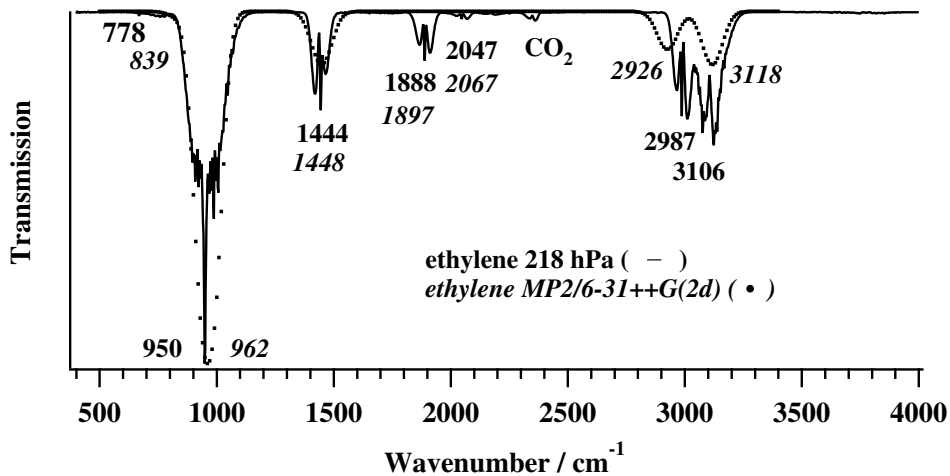
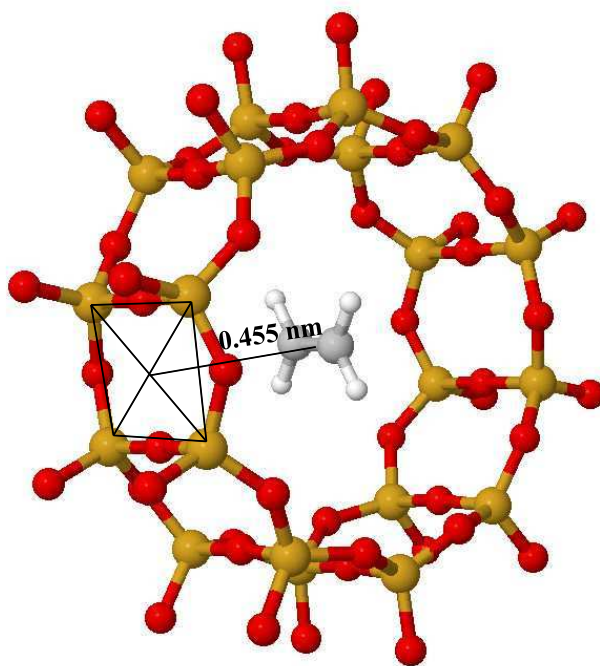


Fig. 4



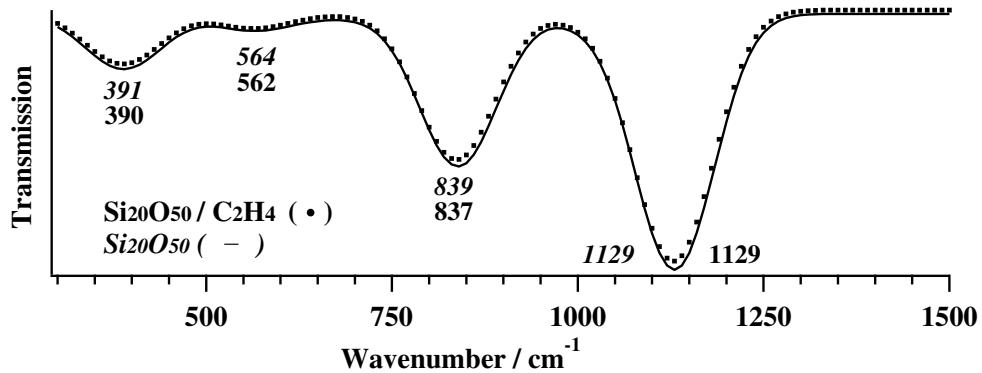
Review Only

Fig. 5



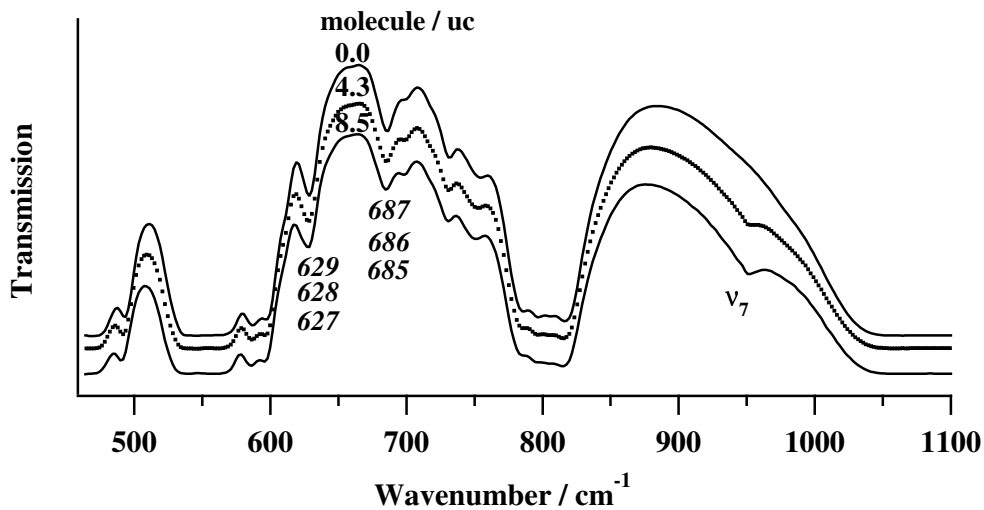
1  
2  
3  
4  
5  
6  
7  
8  
9  
10  
11  
12  
13  
14  
15  
16  
17  
18  
19  
20  
21  
22  
23  
24  
25  
26  
27  
28  
29  
30  
31  
32  
33  
34  
35  
36  
37  
38  
39  
40  
41  
42  
43  
44  
45  
46  
47  
48  
49  
50  
51  
52  
53  
54  
55  
56  
57  
58  
59  
60

Fig. 6



Peer Review Only

Fig. 7



Review Only

Fig. 8

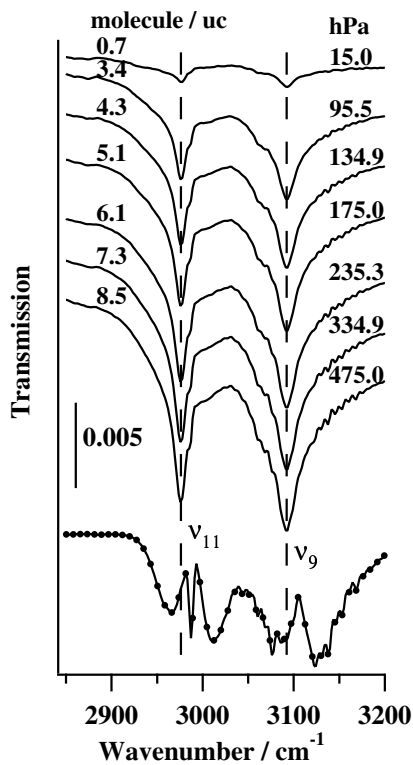


Fig. 9

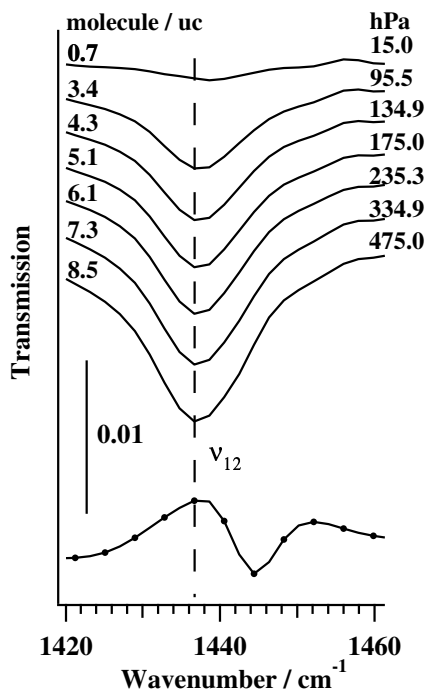
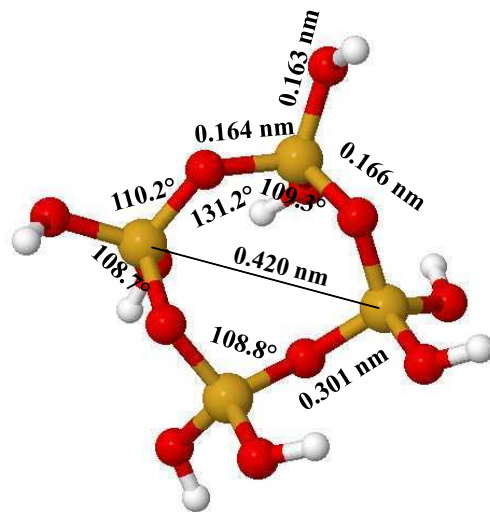


Fig. 10

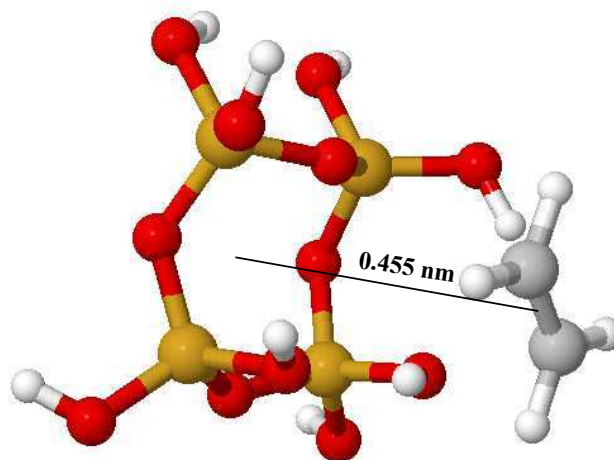


For

2

1  
2  
3  
4  
5  
6  
7  
8  
9  
10  
11  
12  
13  
14  
15  
16  
17  
18  
19  
20  
21  
22  
23  
24  
25  
26  
27  
28  
29  
30  
31  
32  
33  
34  
35  
36  
37  
38  
39  
40  
41  
42  
43  
44  
45  
46  
47  
48  
49  
50  
51  
52  
53  
54  
55  
56  
57  
58  
59  
60

Fig. 11



1  
2  
3  
4  
5  
6  
7  
8  
9  
10  
11  
12  
13  
14  
15  
16  
17  
18  
19  
20  
21  
22  
23  
24  
25  
26  
27  
28  
29  
30  
31  
32  
33  
34  
35  
36  
37  
38  
39  
40  
41  
42  
43  
44  
45  
46  
47  
48  
49  
50  
51  
52  
53  
54  
55  
56  
57  
58  
59  
60

Fig. 12

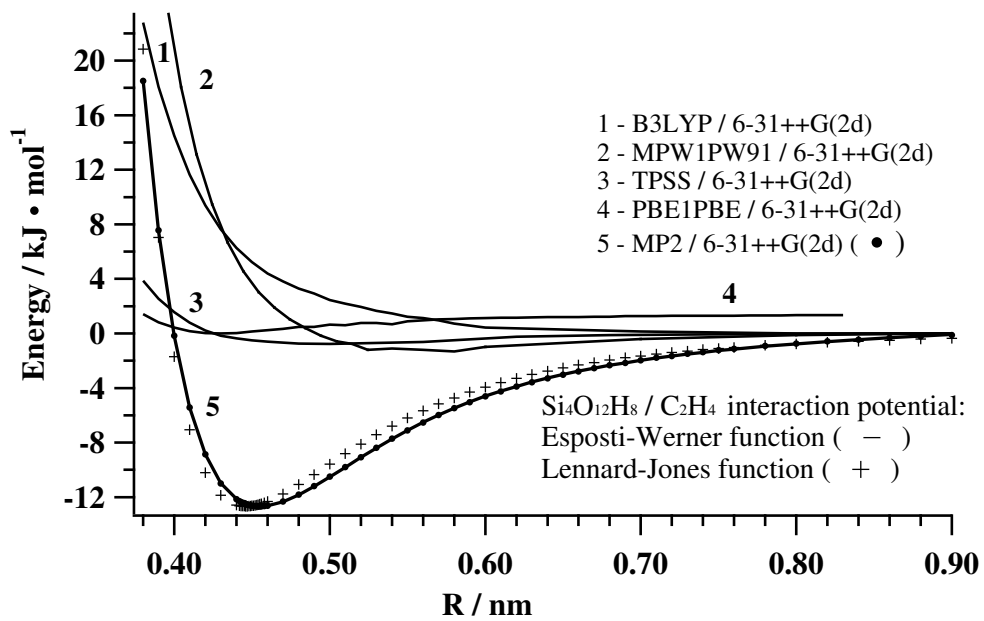


Table 1. Positions of silicalite vibration bands in  $\text{cm}^{-1}$ : experimental (Exp.) measurements and comparison with Molecular Dynamics (MD) and Restricted Hartee-Fock (RHF/3-21G\*\*) calculations (Calc.) with scaling factor.

Vibr. type*	Overtone bands	$\nu_{as.}(\text{O-Si-O})$	$\nu_{as.}(\text{Si-O-Si})$	$\delta(\text{O-Si-O})/(\text{Si-O})_{edge}$	$\nu_s(\text{Si-O-Si})$	Complex bands	$\delta(\text{O-Si-O})$
Exp.(this work)	2023 1892	1240	1089	—	806	686 629 588 569 548	442
Calc. (RHF/3-21G**)			1129	1017 <sup>weak</sup>	839	710 654 563	391
Calc. (MD)		1203	1203	—	815	582	499

\* - According to the classification of Flanigen [35].

TABLES

35

Table 2. Harmonic ( $\omega_i$ ) and anharmonic ( $\nu_i$ ) wavenumbers in  $\text{cm}^{-1}$  and calculated related intensities  $I_i$  in  $\text{km/mol}$  (in parentheses) of the ethylene molecule: RHF/6-31++G(2d) and Møller-Plesset (MP2/6-31++G(2d)) calculations (Calc.) and comparison with experimental (Exp.) measurements.

		RHF/6-31++G(2d)	MP2/6-31++G(2d)	Exp.
Mode	Symmetry	$\omega_i (I_i)/\nu_i$	$\omega_i (I_i)/\nu_i$	$\omega_i [37]/\omega_i [38]/\nu_i [43]$
1	$A_g$ symm. CH stretch	3277 (0)/3160	3156(0)/3024	3153/3156/3022
2	$A_g$ CC stretch	1821 (0)/1792	1678(0)/1617	1655/1656/1625
3	$A_g$ symm. HCH bend	1480 (0)/1456	1390(0)/1362	1370/1372/1344
4	$A_u$ $H_2C - CH_2$ twist	1136/(0) 1113	1065(0)/1042	1044/1045/1026
5	$B_{3g}$ CH trans. stretch	3332 (0)/3213	3230(0)/3094	3232/3207/3083
6	$B_{3g}$ HCH anti. wag.	1342 (0)/1320	1261(0)/1236	1245/1249/1222
7	$B_{3u}$ sym. HCH bend out of plane	1072 (123)/1055	985(118)/962	969/968/949
8	$B_{2g}$ anti. HCH bend out of plane	1077 (0)/1056	945(0)/938	959/960/940
9	$B_{2u}$ <i>cis</i> CH stretch	3362 (25)/3234	3257(10)/3118	3234/3239/3105
10	$B_{2u}$ sym. HCH in plane	889 (0)/888	844(1)/839	843/844/826
11	$B_{1u}$ anti. CH stretch	3254 (19)/3126	3139(7)/2926	3147/3130/2989
12	$B_{1u}$ anti. HCH bend in plane	1593 (9)/1559	1484(10)/1448	1473/1472/1443

Table 3. Position of  $(\nu_i + \nu_j)$  combination and  $2\nu_i$  overtones bands in  $\text{cm}^{-1}$  for the ethylene molecule: Møller-Plesset (MP2/6-31++G(2d)) calculations (Calc.) and comparison with experimental (Exp.) measurements.

Band	MP2/6 - 31 + +G(2d)	Exp.[43]	Band	MP2/6 - 31 + +G(2d)	Exp.[43]
$\nu_8 + \nu_{10}$	1776	1767	$2\nu_{10}$	1702	1662
$\nu_7 + \nu_{10}$	1806	1781	$2\nu_8$	1893	1881
$\nu_4 + \nu_{10}$	1882	1854	$2\nu_7$	1923	1900
$\nu_7 + \nu_8$	1897	1889	$2\nu_4$	2082	2046
$\nu_4 + \nu_8$	1976	1958	$2\nu_3$	2721	2685
$\nu_4 + \nu_7$	1996	1965	$2\nu_{12}$	2891	2877
$\nu_6 + \nu_{10}$	2067	2048	$2\nu_2$	3231	3239
$\nu_3 + \nu_{10}$	2202	2173	$2\nu_{11}$	5826	5939
$\nu_3 + \nu_7$	2321	2292	$2\nu_9$	6205	6197
$\nu_2 + \nu_{10}$	2418	2439	$\nu_5 + \nu_6$	4329	4310
$\nu_2 + \nu_7$	2572	2571	$\nu_6 + \nu_9$	4347	4322
$\nu_2 + \nu_3$	2970	2962	$\nu_3 + \nu_{11}$	4282	4329
$\nu_2 + \nu_{12}$	3146	3079	$\nu_{11} + \nu_{12}$	4278	4408
$\nu_{10} + \nu_{11}$	3761	3809	$\nu_3 + \nu_9$	4472	4440
$\nu_1 + \nu_{10}$	3860	3842	$\nu_1 + \nu_{12}$	4470	4460
$\nu_8 + \nu_{11}$	3856	3921	$\nu_5 + \nu_{12}$	4531	4515
$\nu_9 + \nu_{10}$	3954	3928	$\nu_2 + \nu_{11}$	4451	4597
$\nu_7 + \nu_{11}$	3883	3931	$\nu_1 + \nu_2$	4622	4632
$\nu_1 + \nu_8$	3955	3954	$\nu_2 + \nu_9$	4733	4730
$\nu_7 + \nu_9$	4071	4047	$\nu_1 + \nu_{11}$	5898	5995
$\nu_6 + \nu_{11}$	4156	4207	$\nu_5 + \nu_{11}$	6150	6151

Table 4. Assignment and position of fundamental and combination vibration bands in  $\text{cm}^{-1}$  for ethylene: Møller-Plesset (MP2/6-31++G(2d)) and Molecular Dynamics (MD) calculations (Calc.) comparison with experimental (Exp.) data for the gas phase at 218 hPa.

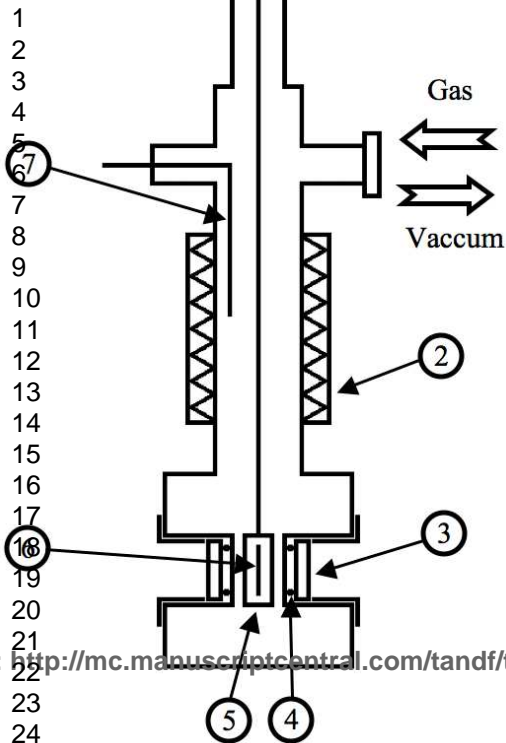
Vibration modes	MP2/6-31++G(2d)	Exp. (this work)	MD[8]
$\nu_7$	962	950	981
$\nu_7 + \nu_8$	1897	1888	—
$\nu_6 + \nu_{10}$	2067	2047	—
$\nu_9$	3118	3106	3129
$\nu_{10}$	839	778 ( <i>P</i> -branch)	—
$\nu_{11}$	2926	2987	3020
$\nu_{12}$	1448	1444	1467

Table 5. Harmonic ( $\omega_{ads}$ ) wavenumbers in  $\text{cm}^{-1}$ , harmonic ( $\Delta\omega = \omega_{ads} - \omega_{gas}$ ) wavenumber shifts in  $\text{cm}^{-1}$  and related intensities in  $\text{km/mol}$  (in parentheses) for the ethylene molecule adsorbed (ads) in the  $\text{Si}_{20}\text{O}_{50}$  cluster and the ethylene molecule alone (gas), calculated at the RHF level of theory using the 3-21G\*\* basis set (with scaling factor), and for the ethylene molecule adsorbed on the  $\text{Si}_4\text{O}_{12}\text{H}_8$  fragment and the molecule ethylene alone (gas), calculated at the MP2 level of theory using 6-31++G(2d) basis set.

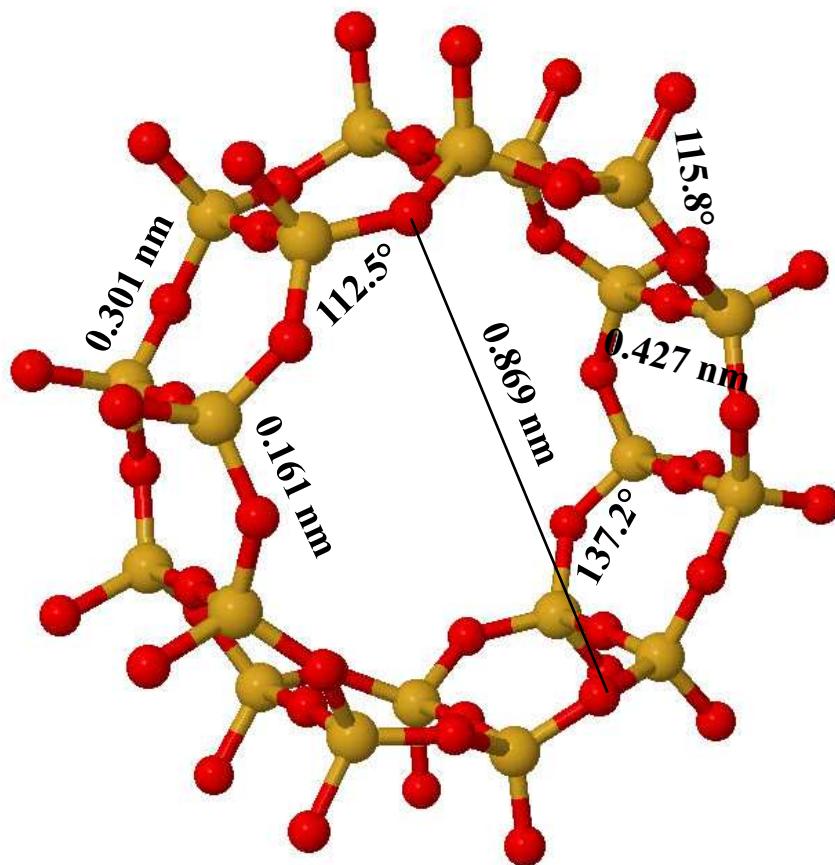
		RHF/3-21G**			MP2/6-31G++G(2d)		
		$\text{Si}_{20}\text{O}_{50}$			$\text{Si}_4\text{O}_{12}\text{H}_8$		
Mode	Sym.	$\omega_{ads}$	$\Delta\omega_{calc}/\Delta\nu_{exp}$	$I_{gas}$ ( $I_{ads}$ )	$\omega_{ads}$	$\Delta\omega_{calc}/\Delta\nu_{exp}$	$I_{gas}$ ( $I_{ads}$ )
1	$A_g$	3075	-8	0(0)	3156	0	0(0)
2	$A_g$	1650	-10	0(0)	1673	-5	0(0)
3	$A_g$	1360	-6	0(0)	1386	-4	0(0)
4	$A_u$	1056	2	0(0)	1066	-1	0(136)
5	$B_{3g}$	3123	-10	0(2)	3231	0.5	0(0)
6	$B_{3g}$	1228	-7	0(0)	1256	-5	0(0)
7	$B_{3u}$	1022	17	116(81)	984	-1	118(46)
8	$B_{2g}$	1042	12	0(0)	941	-4	0(129)
9	$B_{2u}$	3150	-10/-12	29(29)	3258	1/-12	10(8)
10	$B_{2u}$	836	-3	1(779)	838	-6	1(4)
11	$B_{1u}$	3056	-8/-11	13(2)	3139	0/-11	7(6)
12	$B_{1u}$	1466	4/-8	10(9)	1478	-6/-8	10(10)

Table 6. Harmonic ( $\omega_i$ ) wavenumbers in  $\text{cm}^{-1}$  and related intensities  $I_i$  in  $\text{km/mol}$  (in parentheses) corresponding to T - O stretching and bending for the  $\text{Si}_4\text{O}_{12}\text{H}_8$  fragment with and without ethylene molecule, calculated at the MP2 level of theory using the 6-31++G(2d) basis set.

Mode	$\omega(\text{Si}_4\text{O}_{12}\text{H}_8)$	$\omega(\text{Si}_4\text{O}_{12}\text{H}_8 + \text{C}_2\text{H}_4)$
O-Si-O(asym.)	1092(1150)	1089(1088)
O-Si-O(sym.)	1051(219)	1051(212)
O-Si-O(asym.)	1044(161)	1042(103)
O-Si-O(asym.)	1018(319)	1017(314)
O-Si-O(asym.)	928(157)	926(150)
O-Si-O(sym.)	808(8)	808(12)
Si-O-Si(sym.)	777(93)	776(107)
O-Si-O bend.	389(112)	389(102)
O-Si-O bend.	400(87)	396(72)
O-Si-O bend.	415(87)	413(109)
O-Si-O bend.	424(44)	424(41)
O-Si-O bend.	437(58)	436(66)
Ring	667(121)	667(119)
Ring	662(91)	662(89)
Ring	590(18)	589(16)
Ring	508(94)	499(73)
Ring	472(48)	472(44)



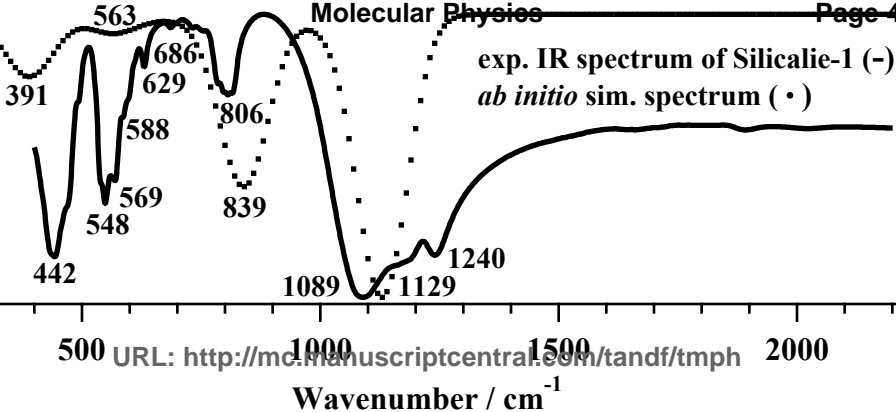
1  
2  
3  
4  
5  
6  
7  
8  
9  
10  
11  
12  
13  
14  
15  
16  
17  
18  
19  
20  
21  
22  
23  
24  
25  
26  
27  
28  
29  
30  
31  
32  
33  
34  
35  
36  
37  
38  
39  
40  
41  
42  
43  
44  
45  
46  
47  
48  
49  
50  
51  
52  
53  
54  
55  
56  
57  
58  
59  
60



Only

exp. IR spectrum of Silicalie-1 (-)  
*ab initio* sim. spectrum (•)

Transmission



500

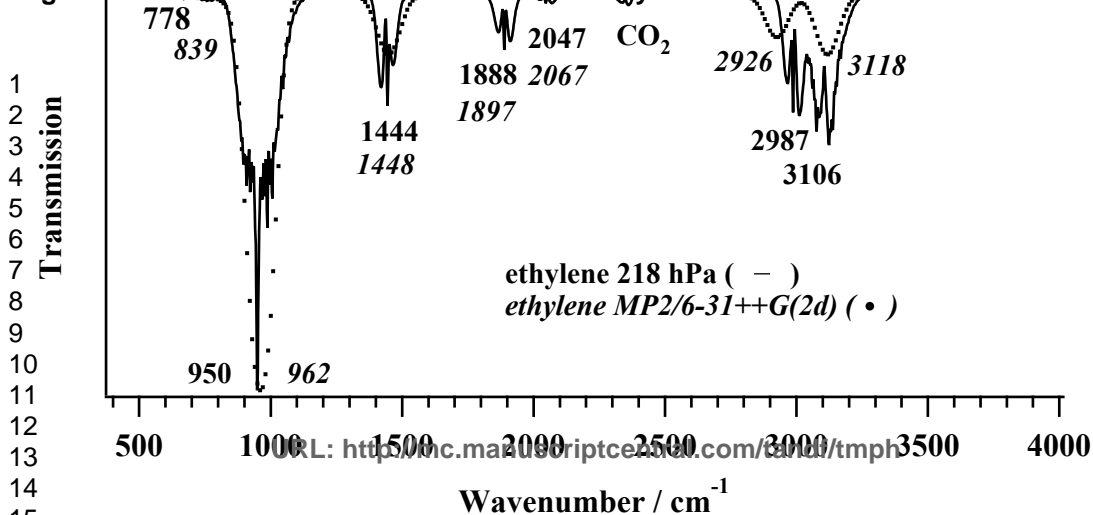
1000

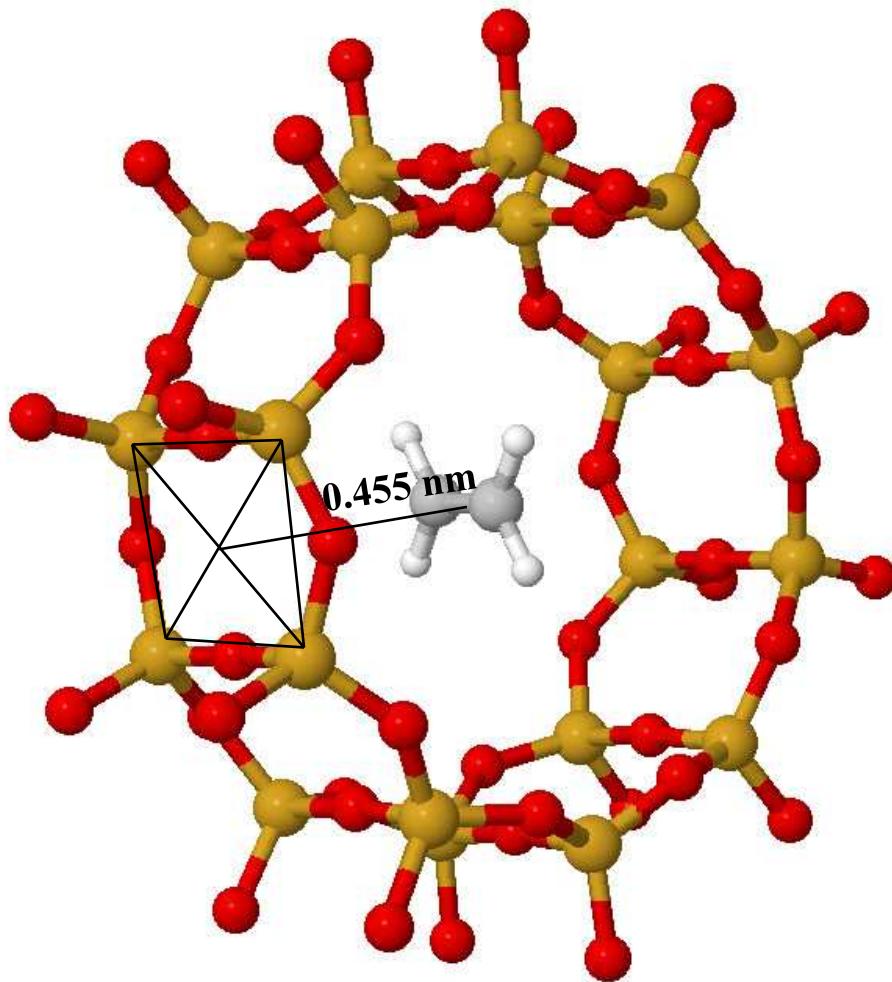
1500

2000

Wavenumber / cm<sup>-1</sup>

URL: <http://mc.manuscriptcentral.com/tandf/temph>





Transmission

391  
390564  
562839  
837 $\text{Si}_{20}\text{O}_{50} / \text{C}_2\text{H}_4$  ( • )  
 $\text{Si}_{20}\text{O}_{50}$  ( - )

1129

1129

500

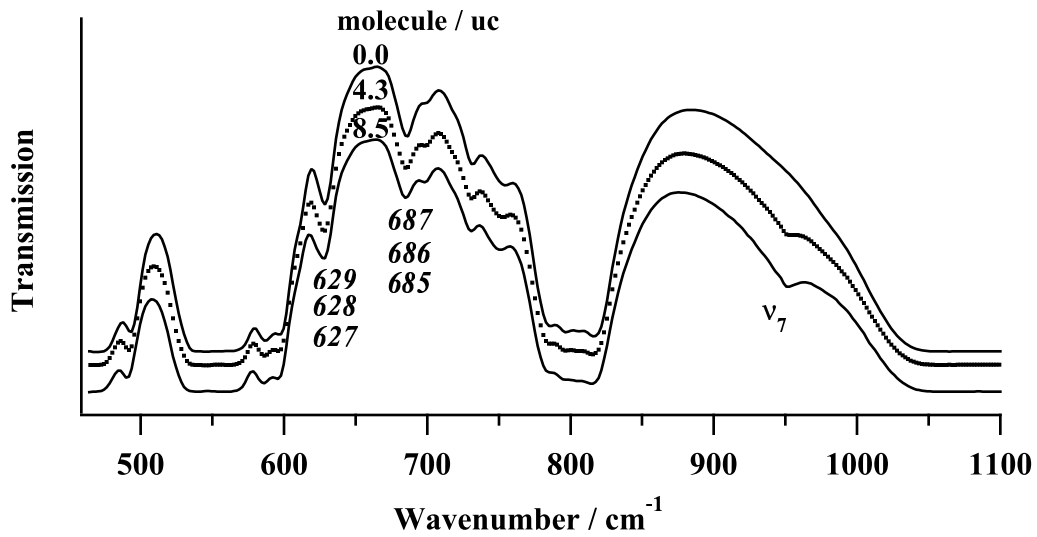
750

1000

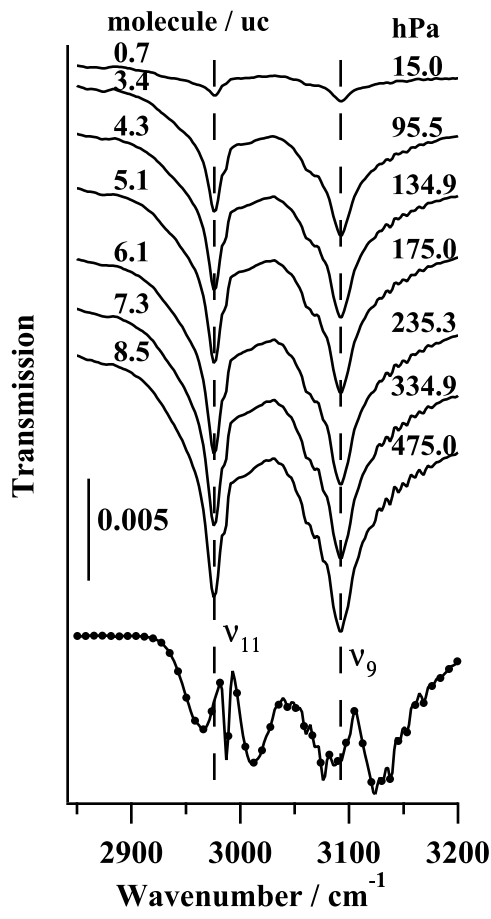
1250

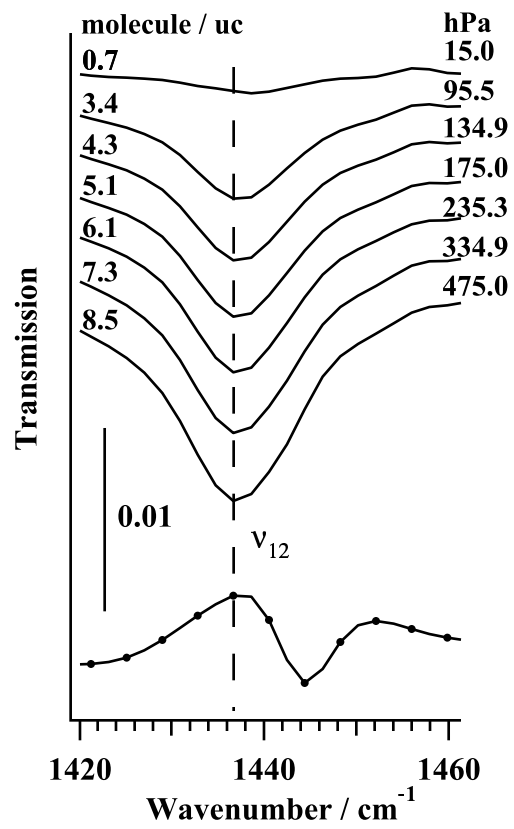
1500

Wavenumber /  $\text{cm}^{-1}$ 1  
2  
3  
4  
5  
6  
7  
8  
9  
10  
11  
12URL: <http://mc.manuscriptcentral.com/tandf/tmph>

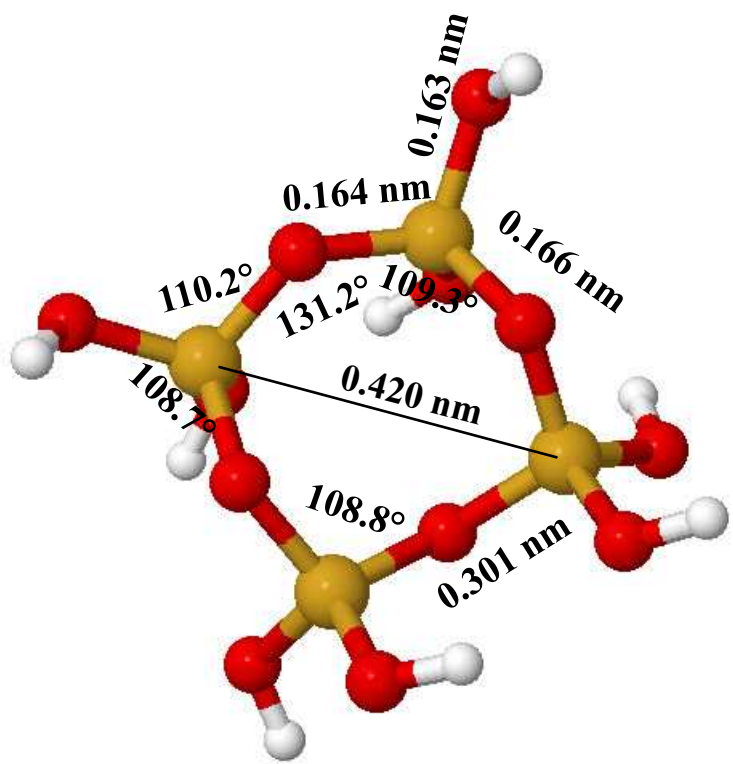


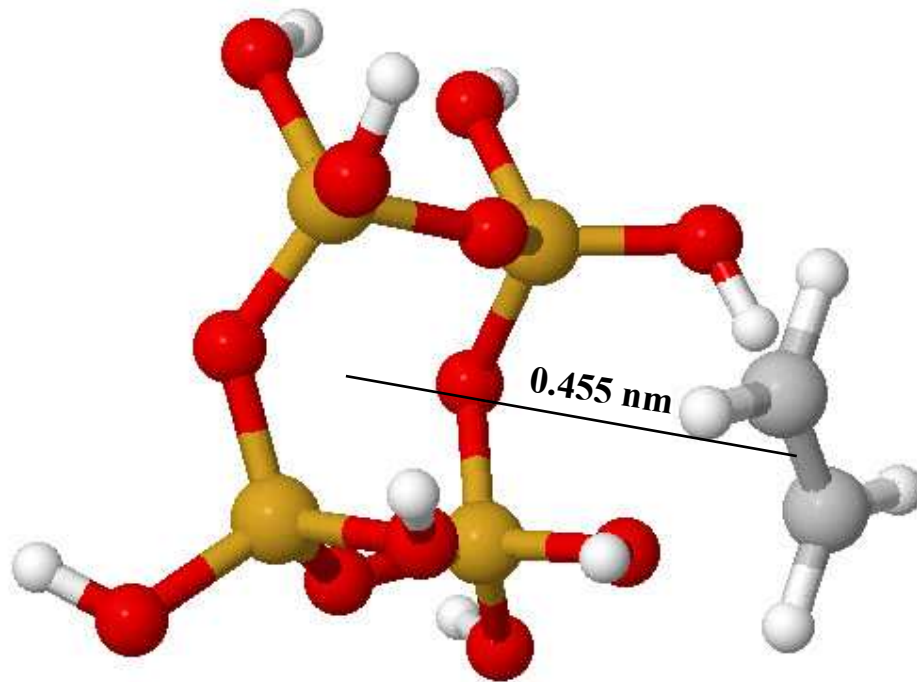
1  
2  
3  
4  
5  
6  
7  
8  
9  
10  
11  
12  
13  
14  
15  
16  
17  
18  
19  
20  
21  
22  
23  
24  
25  
26  
27  
28  
29  
30  
31  
32  
33  
34  
35  
36  
37  
38  
39  
40  
41  
42  
43  
44  
45  
46  
47  
48  
49  
50  
51  
52  
53  
54  
55  
56  
57  
58  
59  
60

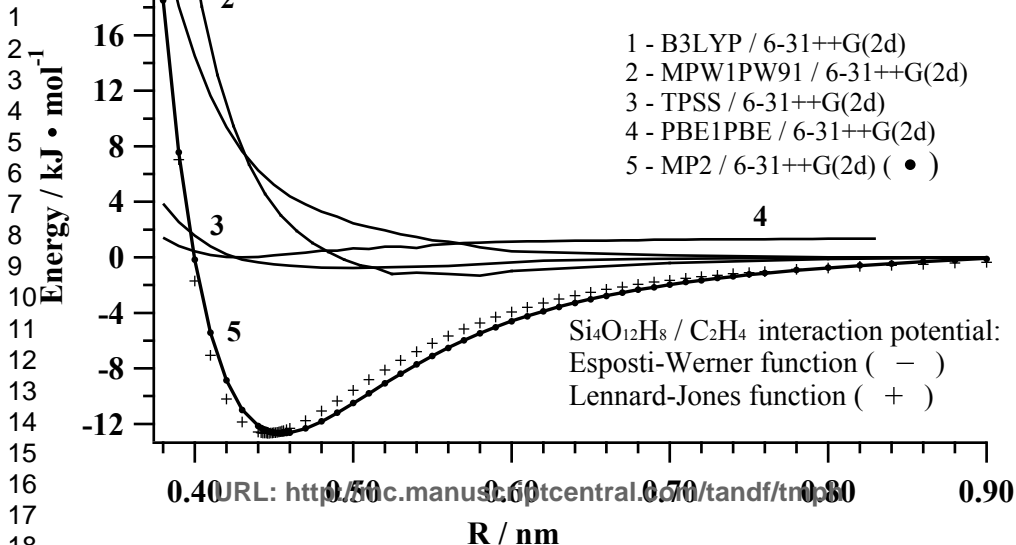




1  
2  
3  
4  
5  
6  
7  
8  
9  
10  
11  
12  
13  
14  
15  
16  
17  
18  
19  
20  
21  
22  
23  
24  
25  
26  
27  
28  
29  
30  
31  
32  
33  
34  
35  
36  
37  
38  
39  
40  
41  
42  
43  
44  
45  
46  
47  
48  
49  
50  
51  
52  
53  
54  
55  
56  
57  
58  
59  
60







URL: <http://sc.manuscriptcentral.com/tandf/tpm>